REPORT DOCUMENTATION PAGE

Form Approved
OMB No. 0704-0188

1. REPORT DATE *(DD-MM-YYYY)*	2. REPORT TYPE	3. DATES COVERED *(From - To)*
30-04-2007	Journal Article	

4. TITLE AND SUBTITLE

Impact of L/D on 90 Degree Sharp-Edge Orifice Flow with Manifold Passage Cross Flow (Preprint)

5a. CONTRACT NUMBER

5b. GRANT NUMBER

5c. PROGRAM ELEMENT NUMBER

6. AUTHOR(S)
W.H. Nurick, T. Ohanian (Science & Technology Applications); D.G. Talley and P.A. Strakey (AFRL/PRSA)

5d. PROJECT NUMBER

5e. TASK NUMBER
50260538

5f. WORK UNIT NUMBER

7. PERFORMING ORGANIZATION NAME(S) AND ADDRESS(ES)

Air Force Research Laboratory (AFMC)
AFRL/PRSA
10 E. Saturn Blvd.
Edwards AFB CA 93524-7680

8. PERFORMING ORGANIZATION REPORT NUMBER

AFRL-PR-ED-JA-2007-256

9. SPONSORING / MONITORING AGENCY NAME(S) AND ADDRESS(ES)

Air Force Research Laboratory (AFMC)
AFRL/PRS
5 Pollux Drive
Edwards AFB CA 93524-7048

10. SPONSOR/MONITOR'S ACRONYM(S)

11. SPONSOR/MONITOR'S NUMBER(S)
AFRL-PR-ED-JA-2007-256

12. DISTRIBUTION / AVAILABILITY STATEMENT

Approved for public release; distribution unlimited (PA #07174A).

13. SUPPLEMENTARY NOTES
Submitted for publication in *Journal of Fluids Engineering*.

14. ABSTRACT

A process model is proposed to explain the various stages of flow conditions that are observed by measurement as the flow transitions from non-cavitation to cavitation (turbulent flow), supercavitation, and finally separation in sharp-edge 90 degree orifices. This study includes orifice L/D from 1 to 10, orifice diameters of nominally 0.048 and 0.078 inch, and upstream pressures from 100 to 1500 psi as well as manifold cross flow velocity of from 6 to 60 ft/sec. The results support two different first order models, one for cavitation and the other non-cavitation in turbulent flow. Under full cavitation conditions the discharge coefficient is related to the contraction coefficient and the cavitation number to the ½ power. In the non-cavitation full flow regime the head loss is related to the loss coefficient and the dynamic pressure at the orifice exit. Both the head loss and contraction coefficient were found to be a strong function of the ratio of upstream velocity-to-orifice exit velocity. The area ratio between the manifold and the orifice were also found to have a significantly influence the contraction coefficient. Relationships are proposed to explain the processes leading to hydraulic flip (separation) and prediction of occurrences that include inception of cavitation, supercavitation, and separation.

15. SUBJECT TERMS

16. SECURITY CLASSIFICATION OF:			17. LIMITATION OF ABSTRACT	18. NUMBER OF PAGES	19a. NAME OF RESPONSIBLE PERSON
a. REPORT	b. ABSTRACT	c. THIS PAGE			Dr. Stephen A. Danczyk
Unclassified	**Unclassified**	**Unclassified**	SAR	35	19b. TELEPHONE NUMBER *(include area code)* N/A

IMPACT OF L/D ON 90 DEGREE SHARP-EDGE ORIFICE FLOW WITH MANIFOLD PASSAGE CROSS FLOW (Preprint)

By:

W. H. Nurick & T. Ohanian
Science & Technology Applications, LLC (STA)
Moorpark, CA

And

D.G. Talley & P. A. Strakey
Air Force Research Laboratory
Edwards Air Force Base CA

ABSTRACT

A process model is proposed to explain the various stages of flow conditions that are observed by measurement as the flow transitions from non-cavitation to cavitation (turbulent flow), supercavitation, and finally separation in sharp-edge 90 degree orifices. This study includes orifice L/D from 1 to 10, orifice diameters of nominally 0.048 and 0.078 inch, and upstream pressures from 100 to 1500 psi as well as manifold cross flow velocity of from 6 to 60 ft/sec. The results support two different first order models, one for cavitation and the other non-cavitation in turbulent flow. Under full cavitation conditions the discharge coefficient is related to the contraction coefficient and the cavitation number to the ½ power. In the non-cavitation full flow regime the head loss is related to the loss coefficient and the dynamic pressure at the orifice exit. Both the head loss and contraction coefficient were found to be a strong function of the ratio of upstream velocity-to-orifice exit velocity. The area ratio between the manifold and the orifice were also found to have a significantly influence the contraction coefficient. Relationships are proposed to explain the processes leading to hydraulic flip (separation) and prediction of occurrences that include inception of cavitation, supercavitation, and separation.

INTRODUCTION

Rocket engines operate at both sea level (SL) and vacuum environments. Depending on mission requirements the engine may also be required to startup and/or restart in space. Conditions at both SL and space result in operation during startup within the cavitation regime for injector designs incorporating sharp-edge orifices. Orifice cavitation can cause damage to the thrust chamber and injector due to unacceptable jet characteristics (i.e. misimpingement of impinging jets, jet wall impingement, and/or initiation of combustion instability). Cavitation under these conditions can be controlled by tailoring the startup sequence (upstream pressure/orifice pressure drop) or design of injector elements that avoid cavitation at all operating conditions (i.e. rounded entrances). It is the responsibility of the injector design engineer to ensure that the injector operates at acceptable conditions under all operating conditions. In order to accomplish this a-priori rather than use cut-and-try, the design engineer must have design information for (1) predicting manifold/orifice flow characteristics in both the non-cavitation and cavitation regimes and (2) the resulting impact on jet and flow characteristics. To date this type of information has been limited or nonexistent.

Recognizing this need the US Air Force Research Propulsion Laboratory at Edwards Air Force Base, California initiated a broad study of orifice flow in both the cavitation and non-cavitation regime, in a unique experimental facility, using a range of impinging injector element design variables consistent with rocket engine design. Results from this facility were published by Strakey and Talley[1] in 1999.

This paper describes the results from 90 degree sharp-edge orifices with manifold feeder cross flow from 6 to 60 ft/sec, L/D from 1 to 10 and two orifice sizes (nominally 0.048 and 0.078 inch). The results of this study provide an engineering process for determining the flow regime and analysis method for defining the pertinent flow variables.

COLD FLOW INJECTOR CHARACTERIZATION FACILITY

FACILITY DESIGN

The experimental investigation was carried out at the Air Force Research Laboratory cold-flow injector characterization facility, a simplified schematic of which is shown in Figure 1. Water, which is used as a simulant for liquid oxygen, is stored and pressurized in a 35 ft^3 tank. The injector inlet flow rate is controlled with a throttling valve and measured with one of several turbine flow meters arranged in parallel to cover a wide range of flow rates. Downstream of the injector, another turbine flow meter measures the outlet flow rate and a back-pressure regulator maintains the injector fluid pressure. Fluid pressures of up to 1500 lb/in^2 and manifold velocities up to 130 f/s may be produced in this manner. The injector, as illustrated in Figure 2, consists of an interchangeable stainless steel plate with a sharp-edged hole machined in the center of the plate. This is mounted against the fluid manifold, which contains a 0.25 in square channel machined into the manifold. A plenum and screen at the inlet and exit of the manifold reduces the velocity before the flow enters the manifold in order to generate a reproducible flow field

at the entrance to the orifice. The distance from the manifold inlet screen to the orifice entrance is 2.5 in or 9 manifold channel widths. The entire arrangement is secured inside an optically accessible pressure chamber which is rated to 2000 psi.

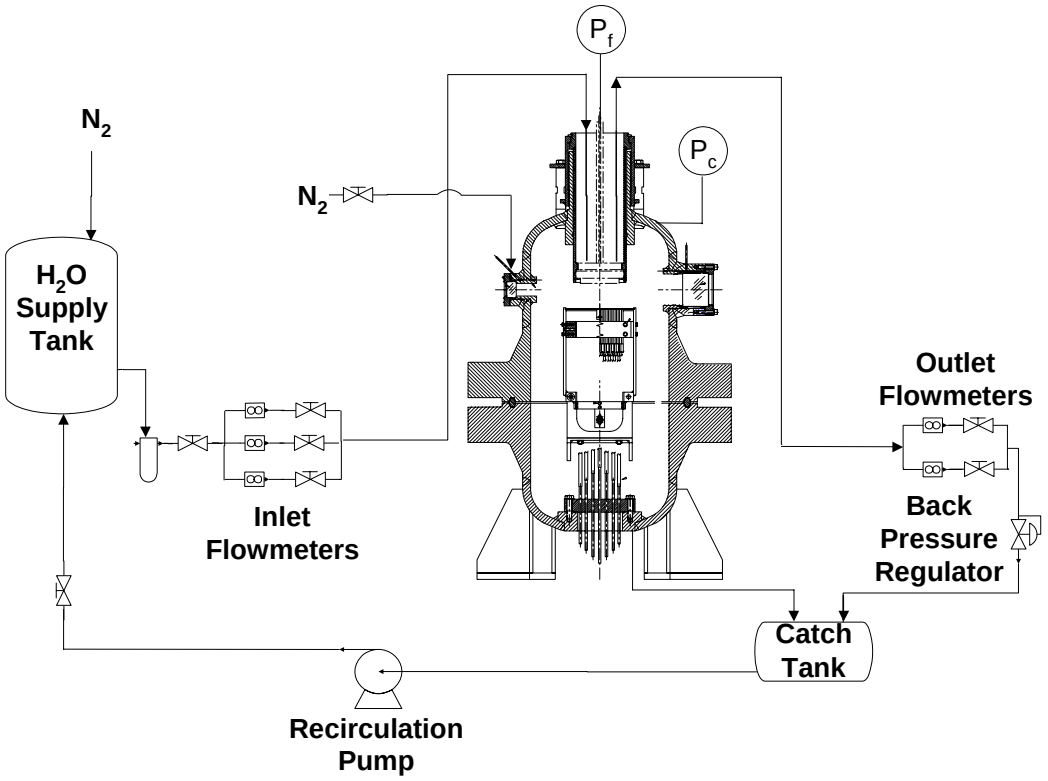

Figure 1 - Schematic of AFRL Cold Flow Test Facility

The orifices are either pilot drilled and reamed, or made by electrical discharge machining with a diameter tolerance of +/- 13 μm and inlet edge radius to orifice diameter ratio of less than .003, ensuring a sharp edged inlet. Chamber pressure, orifice pressure-drop, and inlet and outlet flow rates are recorded by a 12 bit analog to digital conversion board and the data is stored on a personal computer. Experiments are typically conducted by setting the fluid pressure and flow rates to a predetermined value, with the chamber pressure being gradually increased while the data acquisition system records flow rates and pressures. This allows for a large amount of data to be collected in a relatively short period of time. Orifice pressure drop and chamber gas pressure are measured within an accuracy of +/- 0.25%. Manifold velocities are held constant to within +/- 1.5% during the experiment. Because of the difficulty associated with directly

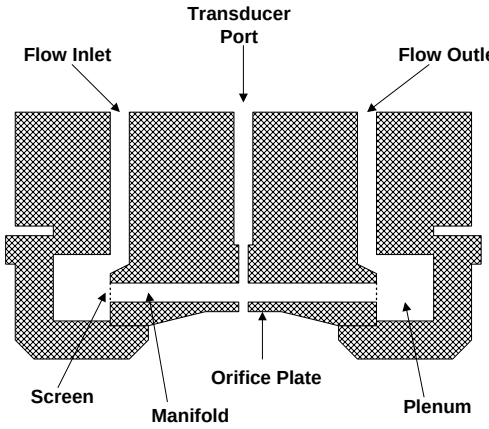

Figure 2 - Injector Schematic

measuring the orifice flow rate inside of the pressurized vessel, the orifice flow rate is measured by subtracting the manifold outlet flow rate from the manifold inlet flow rate. The experimental error associated with the discharge coefficient measurement is limited by the accuracy of the flow meters which is +/- 0.5%. This translates to an error on the discharge coefficient data of about +/- 0.5% at the lowest manifold flow rates and highest orifice flow rates, to +/- 10% at the lowest orifice flow rates and highest manifold flows. A typical error for the intermediate flow rates is on the order of +/- 4%.

The range of operating conditions and orifice geometries typical of liquid rocket injectors was studied and are given in Table 1.

Table 1 - Test Variables and Range of Testing

Orifice Diameter (in)	0.0468 - .0839
Length to Diameter Ratio	3 - 10
Fluid Pressure (psi)	100 - 1500
Back-Pressure (psi)	13.05 - 1500
Cross-Velocity (f/s)	0 – 60.7
Orifice Re_d	$1.0x10^4$ - $3.0x10^5$
Manifold Re_w	$6.0x10^3$
Manifold Dynamic Head to Orifice Static Dp Ratio	$5.0x10^{-5}$ - $6.0x10^0$

MANIFOLD CONFIGURATIONS TESTED

Tests were conducted to distinguish between flow that: (1) entered a manifold from both ends and then contracted to enter a 90 degree sharp-edge orifice (Configuration # 1), (2) entered the manifold from one end and contracted to enter a 90 degree sharp edge orifice (Configuration # 2), and (3) entered the manifold from one end and part of the flow contracted to enter a 90 degree sharp edge orifice and the remainder exited through the manifold exit (Configuration #3). A sketch of the configurations is shown in Figure 3.

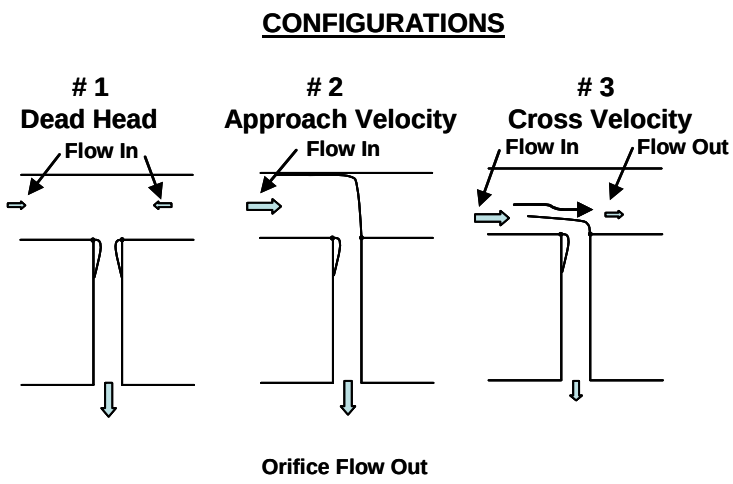

Figure 3 - Orifice Entrance Test Configurations

For Configuration # 1 and #2 the ratio between the velocity V_1 of the manifold inlet and the orifice exit velocity V_2 is constant and equal to the ratio between the orifice area A_2 and the manifold area A_1. This remains true for Configuration #3, but in that case the area $A_1$is to be interpreted to be the cross sectional area only of the flow that enters the orifice, not the entire area of the manifold. This later case therefore introduces another independent variable not present in the first two configurations.

ANALYSIS APPROACH

CAVITATION TURBULENT FLOW

To account for all the dynamic variables in the flow, the analysis below is carried out in terms of the following dimensionless variables: the area ratio A_1/A_2, the velocity ratios V_1/V_2, $(V_1-V_{out})/V_2$ for Configuration #3, where Vout is the manifold exit velocity, the discharge coefficient C_d, the contraction coefficient C_c, and the cavitation number K_{cav}. The discharge coefficient is defined to be the ratio of the actual flowrate to the ideal flowrate. The contraction coefficient is defined to be the ratio of the area of the vena-contracta A_c to the exit area A_2. The cavitation number is defined as:

$$K_{cav} = \frac{P_1 - P_v}{P_1 - P_2} \qquad (1)$$

P_1 is the manifold pressure, P_2 is the backpressure at the orifice exit, and P_V is the liquid vapor pressure. The derivation of relationships between these dimensionless variables depends on various assumptions unique to the flow characteristics of the configurations tested.

In-Line Orifices

The classic textbook case concerns in-line orifices where V_1 and V_2 both flow in the same direction and no bulk flow turning occurs. Furthermore, V_1 is assumed small and can be neglected. The discharge coefficient is then defined as:

$$C_d = \frac{V_2}{\left[(2g/\rho)(P_1 - P_2)\right]^{1/2}} \qquad (2)$$

Combining Equations 1 and 2 results in:

$$C_d = \frac{K_{cav}{}^{1/2} V_2}{\left[(2g/\rho)(P_1 - P_v)\right]^{1/2}} \qquad (3)$$

For this configuration the Bernoulli equation together with Equations 4 and 5 results in Equation 6:

$$C_c = \frac{V_2}{V_c} \qquad (4)$$

$$V_c = \frac{V_1 A_1}{A_2 C_c} \qquad (5)$$

$$C_d = \frac{C_c (K_{cav})^{1/2}}{\left[1 - \left(\frac{A_2}{A_1}\right)^2 Cc^2\right]^{1/2}} \qquad (6)$$

It should be noted that the assumption made in the application of the Bernoulli Equation is that at cavitation, the vena-contracta static pressure is:

$$P_v \approx P_c \qquad (7)$$

And that the H_L term between the manifold and the vena contracta is small.

Neglecting the manifold velocity implies that the ratio A_2/A_1 is small and that the second expression in the denominator of Equation (6) is small with respect to 1. Then for engineering purposes Equation 6 reduces to:

$$C_d = C_c (K_{cav})^{1/2} \qquad (8)$$

This is the expression used in Nurick[2] and subsequent studies[3-10] for In-Line orifices and found to represent the data.

Configuration #1

For all three configurations considered in the present study V_1 could not be assumed to be negligible and therefore it must be included in the determination of C_d. For Configuration #1 and #2 the resulting expression for the discharge coefficient is:

$$C_d = \frac{V_2}{\left[(2g/\rho)(P_1 - P_2) + V_1^{\,2}\right]^{1/2}} \qquad (9)$$

And combining Equations 1, 4, 5, and the Bernoulli Equation results in the expression showed in Equation 10:

$$C_d = \frac{C_c K_{cav}^{\,1/2}}{\left[1 + \left(\frac{A_2}{A_1}\right)^2 C_c^{\,2}\left(K_{cav} - 1\right)\right]^{1/2}} \qquad (10)$$

Note that inclusion of the manifold velocity accounts for the additional K_{cav} term in Equation 10. Further, it was assumed in the derivation that the major head loss is downstream of the vena-contracta, as was assumed for the In-Line orifices. For the designs investigated in this study the denominator for configuration #1 and #2 vary by less than 1 % and therefore Equation 10 could be reduced to that of Equation 8. Equation 10 was, however, used to define the C_d relationship.

The data shown in Figure 4 is typical of the results from Configuration # 1 testing using Equation 10. Note that a straight line may be fitted through the data in the manner of Equation 8 with a slope of 0.6168 and a correlation coefficient R^2 of 0.9999. Since the head loss varies as V_2^2 it would be expected that if significant the curve would not be linear. The linear curve, therefore, confirms that exclusion of the head loss term in Equation 10 does not impact the functional relationship. Figure 4 also supports that the impact of V_1 is negligible and identifies the head loss post vent-contracta as the major head loss area for this configuration.

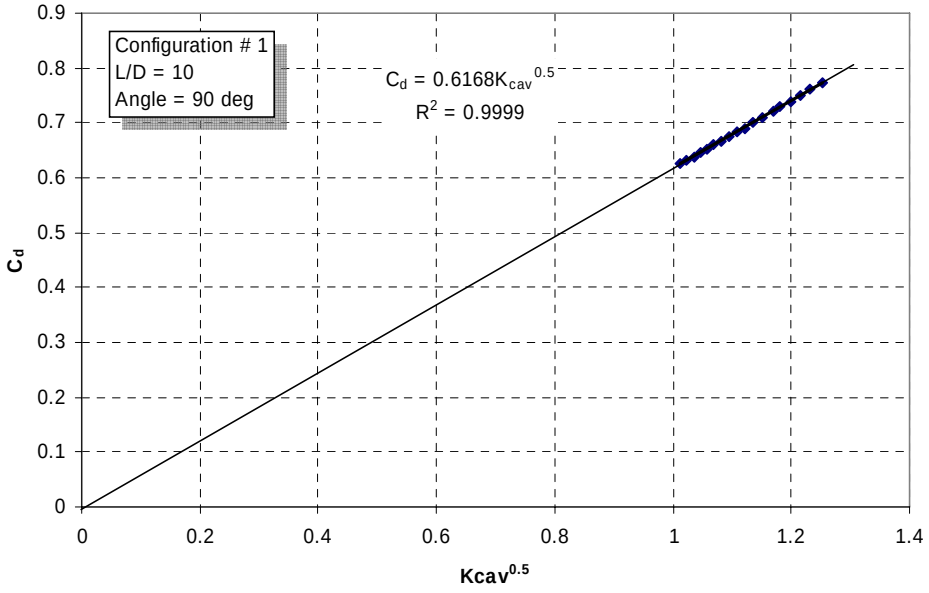

Figure 4 –Relationship between C_d, C_c, and K_{cav} for Configuration #1

Configuration #2

In this configuration all the flow turns 90 deg from one direction. These turning losses can be significant if the flow stagnates against a wall before turning into the orifice (i.e. for 90 degree bends up to 0.75 times the kinetic head[11]). In Configuration #2, where no wall exists, the flow does not stagnate but smoothly turns to flow into the orifice. This results in a significant reduction in the turning losses (i.e. similar to a smooth bend[12]). Consequently, it was initially assumed that Equation 10 would still be representative of the flow characteristics for this configuration.

Typical results from Configuration #2 are presented in Figure 5. Once again a straight line could be plotted through the data in the manner of Equation 8 with a large correlation coefficient implying, as in configuration #1, that the effect of V_1 as well as the turning losses was negligible.

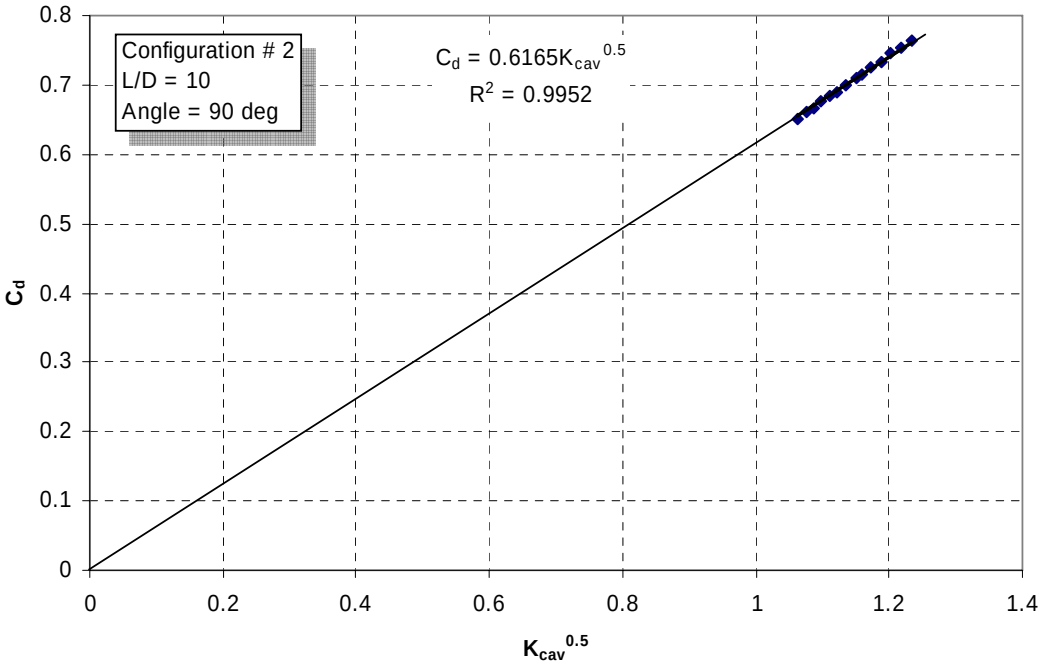

Figure 5 - Relationship between C_d, C_c, and K_{cav} for Configuration #2

Configuration #3

For conditions where the flow entering the manifold exits by two paths, (i.e. the manifold exit and the orifice), and the total pressure in the manifold is constant the discharge coefficient can still be defined by Equation 9. However, Equation 5 then becomes:

$$V_c = \frac{(V_1 - V_{out})}{C_c}\left(\frac{A_1}{A_2}\right) \qquad (11)$$

Utilizing the same equations the resulting discharge coefficient is now defined as:

$$C_d = \frac{C_c K_{cav}^{1/2}}{\left[\frac{(V_1 - V_{out})^2}{V_2^2} \left(\frac{A_1}{A_2} \right)^2 + \left(\frac{V_1}{V_2} \right)^2 C_c^2 (K_{cav} - 1) \right]^{1/2}} \qquad (12)$$

The data were first evaluated using Equation 12 to determine the validity of the assumptions. If the results were found not to be valid then the head loss would be included in the analysis. The data shown in Figure 6 depict the results using Equation 12 for a cross flow velocity of 40 ft/sec and is typical of the data for other cross flow velocities.

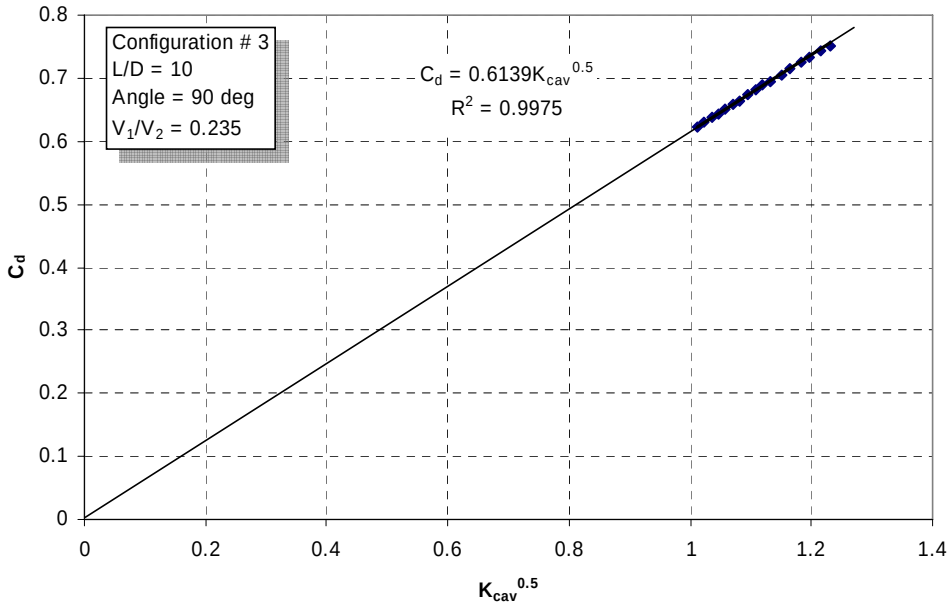

Figure 6 - Relationship between C_d, C_c, and K_{cav}

It was initially thought that the turning losses would be significant and therefore impact head loss. Any impact of K_{cav} and H_L would be revealed by a change in the slope shown in Figure 6, suggesting a variable C_c. The fact that the slope is constant shows that the major head loss is again downstream of the vena-contracta and more importantly that the flow is choked. For all tests, choked flow is indicated by constant flowrate through the orifice in the cavitation regime. It should be noted that each test was run at a specific cross flow resulting in constant velocity ratio.

For any test where the velocity ratio remained constant there was a unique value of C_c (i.e. as defined by Equation 12). However, variations in velocity ratio should impact the vena-contracta formation process and therefore C_c. For Configuration #3, V_1 can be varied for a given orifice flow by simply changing the amount of flow that exits the manifold. This results in a significant change of velocity ratio (between 0.1 and 1). Therefore, determination of C_c for Configuration #3 requires the use on Equation 12 rearranged as:

$$C_c = \frac{\frac{(V_1 - V_{out})}{V_2}\frac{A_1}{A_2}}{\left[\frac{K_{cav}}{C_d^{\,2}} + \left(\frac{V_1}{V_2}\right)^2 (1 - K_{cav})\right]^{1/2}} \qquad (13)$$

Equation 13 was used to define Cc for all Configuration #3 tests.

NON-CAVITATION TURBULENT FLOW

All Configurations

Orifice discharge coefficient in turbulent non-cavitation flow from sharp edge orifices has traditionally been correlated in terms of C_d vs Reynolds number. These correlations have been developed for flow entering the orifice with no cross flow and very low entrance velocity. For configurations where the flow must bend to enter the orifice or contract, researchers[13-14] have typically chosen to correlate head loss (rather than C_d) with the dynamic pressure ($\rho V_2^2/2g$). The correlating constant is termed the loss coefficient (K_L). Therefore, the total head loss for turning constant velocity flow is defined by:

$$H_L = K_L \frac{\rho}{2g} V_2^{\,2} \qquad (14)$$

For conditions where the velocity is not constant then K_L is also be a function of V_1/V_2 or:

$$H_L = K_L\left(\frac{V_1}{V_2}\right)\frac{\rho}{2g} V_2^{\,2} \qquad (15)$$

The head loss can independently be determined using the Bernoulli equation:

$$H_L = (P_1 - P_2) + \frac{\rho}{2g}(V_1^{\,2} - V_2^{\,2}) \qquad (16)$$

The application of Equations 15 and 16 to the specific configurations evaluated define the K_L functionality. In Configurations #1 and #2 the velocity ratio is constant and therefore this variable drops out. For Configuration # 3, K_L is a function of velocity ratio.

FLOW CHARACTERISTICS OF CONFIGURATIONS TESTED

The various stages or regimes of flow encountered in this study are shown in Figure 7. There are 5 regimes and are defined as:

1. Non-Cavitation

2. Cavitation Inception
3. Cavitation with reattachment point moving downstream
4. Supercavitation with quasi-reattachment near or at the orifice exit
5. Separation

All of these stages have been noted by other researchers[3, 7, and 8]. In the test indicated in blue the flow is initially separated (C_d ~ 0.6) then at about a cavitation number of 1.8 ($K_{cav}^{0.5}$ = 1.35) flips to attached flow in the non-cavitation regime. A repeat test indicated in pink starts in the supercavitation regime (quasi-attached) until it quickly transitions to full cavitation, and continues in cavitation until reaching the incipient cavitation point where the flow transitions to non-cavitation. Note that 2 thru 4 above all occur in the cavitation regime. These characteristics are discussed in detail in the following sections.

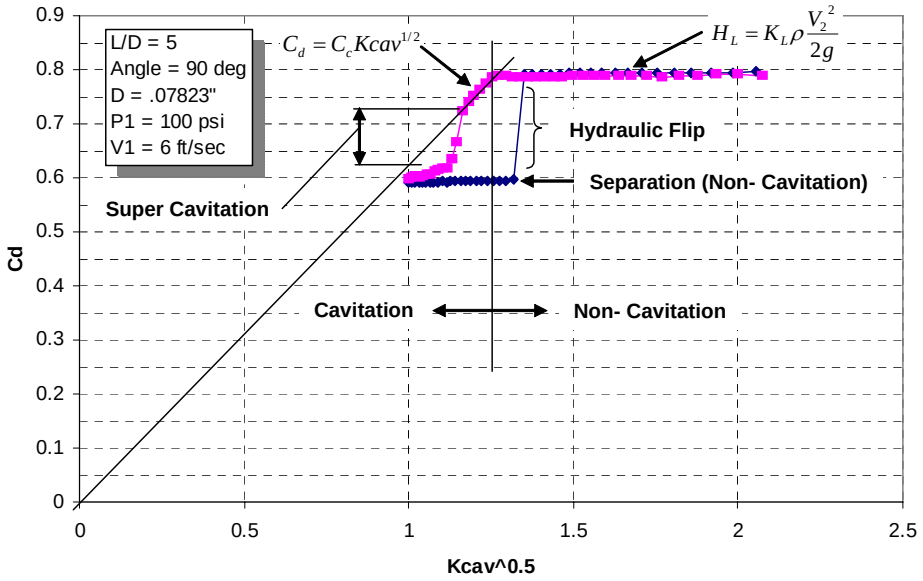

Figure 7 - Results Showing the Various Stages of Flow Characteristics

NON-CAVITATION FLOW REGIME

In the non-cavitation regime the acceleration forces are insufficient to reach vapor pressure in the entry region of the sharp-edge orifice. Nevertheless the accelerating fluid in the core separates from the sharp edge entrance producing a fluid recirculation region between the separation and the reattachment point. The minimum static pressure occurs at the vena-contracta. As the acceleration forces decrease, the core flow area increases and if sufficient orifice length is available reattachment occurs. After reattachment the orifice pressure then decreases at a rate defined primarily by turbulent and friction losses such that the exit pressure matches that of the back pressure. The static pressure and orifice flow characteristics are illustrated below in Figure 8.

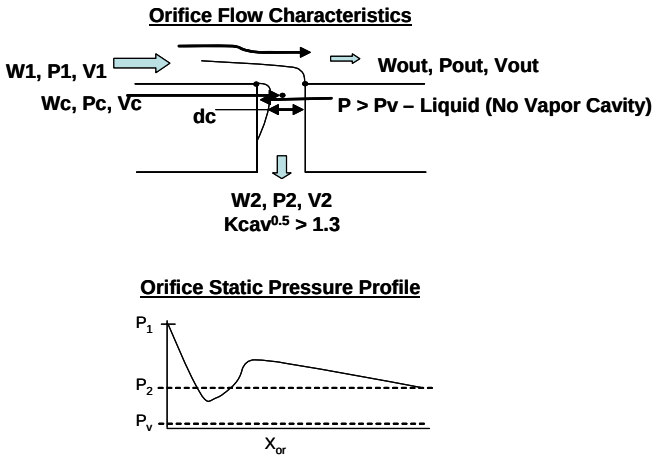

Figure 8 - Illustration of Non-Cavitation Orifice Flow Characteristics

Typical results for the 90 degree sharp edge orifice with Configuration #1 and #2 are presented in Figure 9. Note that the measured loss coefficient for both configurations is only slightly different. The mean deviation of < 0.001 for each curve supports, that for these configurations (i.e. no cross flows), the validity of assumptions in Equation 10.

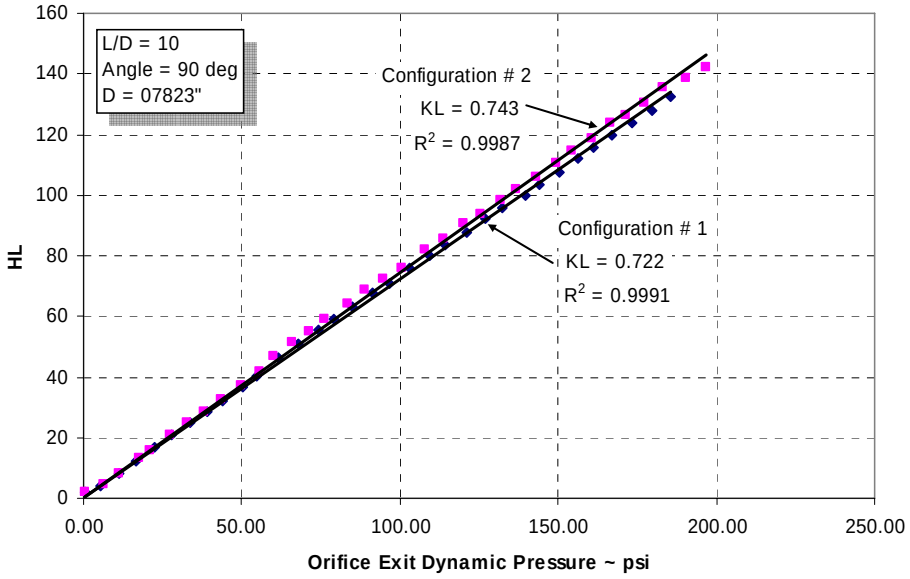

Figure 9 - Head Loss Relationship in Non-Cavitation Turbulent Flow

There is no existing correlation for the 90 degree turning in a cross flow manifold but it would be expected to be near that for a smooth bend (i.e. vanes consistent with Configuration 2) which is 0.2. Based on existing correlations, the head loss coefficient for a contraction of 0.0769 is 0.48. For Configuration # 2 the loss coefficient is only slightly higher (i.e. 0.48+0.2=0.68 vs 0.743) and does not appear to be inconsistent with expectations. Interestingly, KL is 0.75 for a 90 degree elbow at constant velocity[11]. Since the only difference is the contraction, this suggests that the major head loss in non-

cavitation turbulent flow is in turning the flow. It follows then that the major contribution to head loss occurs upstream of the vena-contracta since the turning is complete by that point in the flow.

Typical results for the 90 degree sharp edge orifice with the Cross Flow Configuration #3 are presented in Figure 10. Each data set was conducted at constant velocity ratio even though the inlet manifold velocity varied. Note that the measured loss coefficient varies with manifold velocity and that increasing the velocity causes a greater deviation from the zero intercept. This is a reflection of the impact of V_1/V_2 on K_L. Further, for the cross velocity configuration the loss coefficient, K_L, is constant for any given velocity ratio (V_1/V_2), and the value of K_L varies with velocity ratio. The R^2 fit of the data shows excellent linear correlation. Consequently, K_L will be nonlinear with respect to velocity ratio.

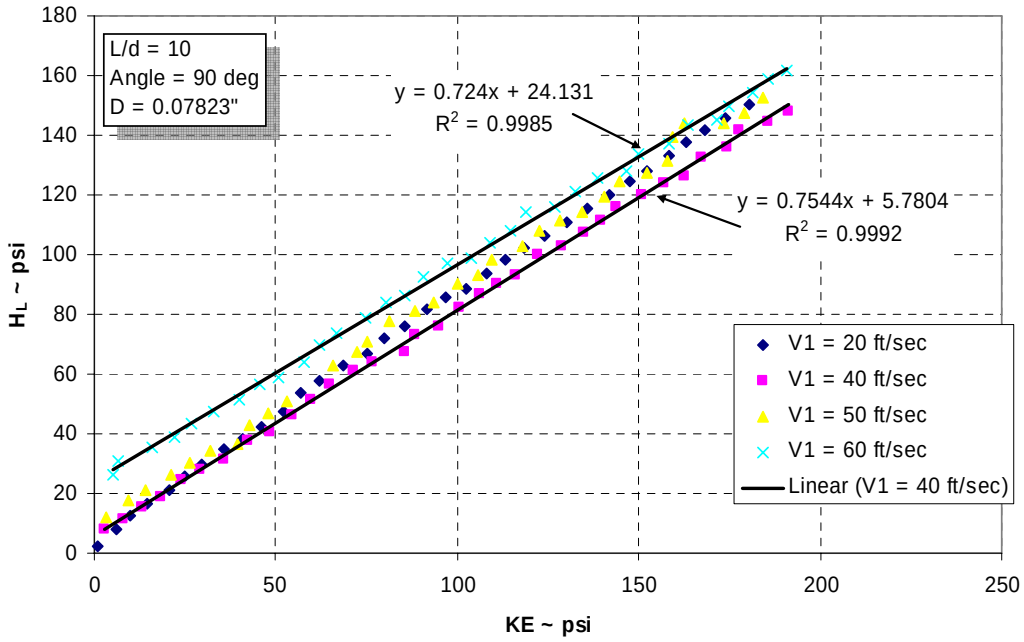

Figure 10 - Head Loss Relationship in Non-Cavitation Turbulent Flow

Data for the 90 degree sharp edge orifice where the velocity ratio varied from ~0.08 to 2.5 and L/D from 1 to 10 are shown in Figure 11 thru 13. For the Cross Velocity configuration, 90 degree sharp edge orifice, the relationship is:

$$K_L = A\left(\frac{V_1}{V_2}\right)^2 + B\left(\frac{V_1}{V_2}\right) + C \qquad (17)$$

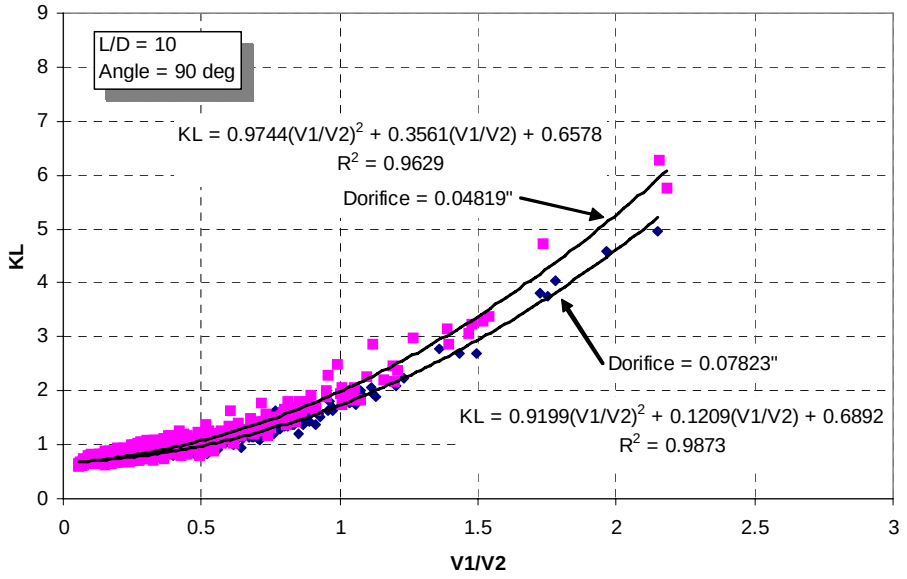

Figure 11 - Correlation of H_L Coefficient for 90 Degree Sharp-Edge Orifice

The constants and R^2 values for all L/D's are shown in their respective Figures.

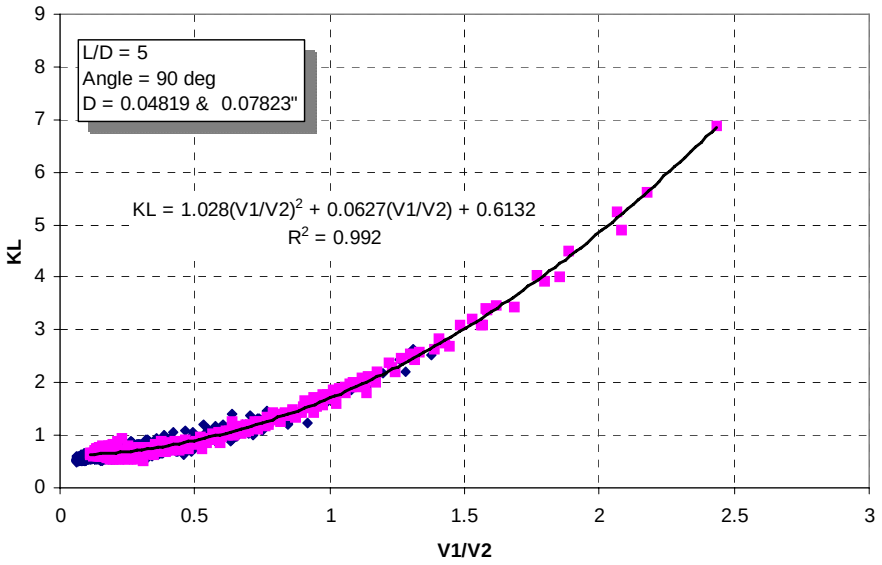

Figure 12 - Correlation of H_L Coefficient for 90 Degree Sharp-Edge Orifice

For the L/D of 2 the data where separation occurred tended to deviate from the single curve at higher velocity ratios. It is believed that this is an artifact of the unstable nature of the flow at this condition and therefore it was not considered in the final correlation.

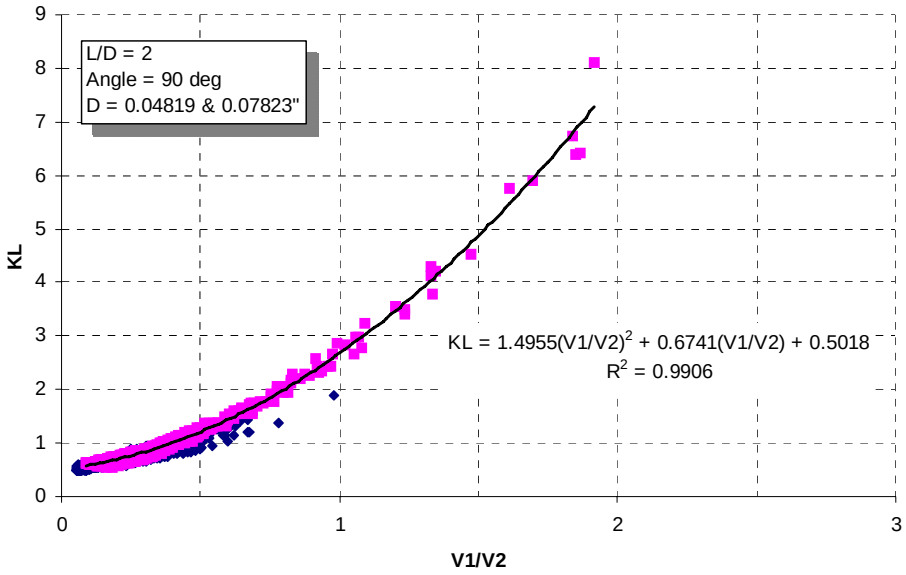

Figure 13 - Correlation of H_L Coefficient for 90 Degree Sharp-Edge Orifice

The results shown in Figures 11-13 are only for attached flow and therefore no data are shown for L/D = 1. Separation did occur at several test conditions for the L/D of 2 and 5 orifices and this variable is discussed in the Separation section of this paper.

INCEPTION OF CAVITATION

As back pressure is lowered, the acceleration forces at the orifice entrance increases, thereby lowering the static pressure. At the point where the onset of cavitation occurs (~ K_{cav} = 1.8), vapor bubbles are observed forming in the boundary layer[8 and 15-19] and C_d starts to decrease as it transitions to full cavitation (i.e. constant C_c and choked flow), Figure 14. Note that the orifice cavity remains at the vapor pressure until the acceleration forces diminish sufficiently for the reattachment process to dominate. After reattachment the flow is similar to that of the non-cavitation characteristics. As the back pressure is further lowered the acceleration forces increase, and depending on the orifice length, either full cavitation or supercavitation occurs.

Koivula[8] noted that at the inception of cavitation the formation and collapse of the bubbles resulted in both a pressure oscillation frequency and overpressure. He found frequencies of 8 KHz at inception of cavitation but low overpressure fluctuations. The low overpressure is thought to be due to the limited number and size of vapor bubbles in this regime.

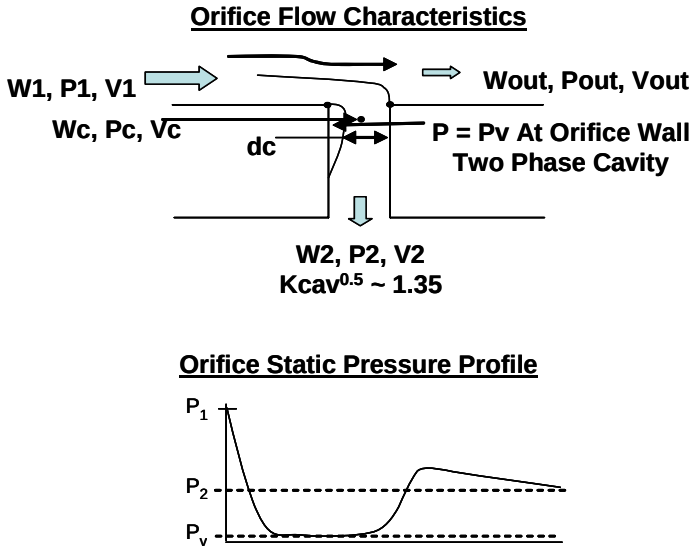

Figure 14 - Illustration showing Pressure Characteristics for Inception of Cavitation

The inception of cavitation is defined as the point where non-cavitation flow transitions into cavitation. This can occur at a point where C_c is immediately constant or transitions to the point where C_c becomes constant. The length of transition depends on the rapidity of generation of bubbles until a vapor cavity forms. Ganippa[3] noted that for an orifice design similar to that of Configuration #1 the generation of vapor bubbles at inception of cavitation occurred completely around the orifice periphery (symmetric), while for Configuration #2 they occurred on the left side (see Figure 14) of the entry at the corner of the orifice entrance and were observed only on that side of the orifice (non-symmetric). In both cases it appeared that the formation of a cavity occurred rapidly as was observed in this study.

The data show that for some conditions there is no bubble formation regime and the flow goes directly from non-cavitation to full cavitation. At other conditions there is a clear distinction between non-cavitation and the Kcav value for full cavitation (i.e. Cc = constant). This is best shown by plotting the flowrate vs Kcav and noting the slope change between the two regimes until the flowrate becomes constant. This change in slope indicates the inception of cavitation and the constant flowrate indicates where full cavitation occurs. At low manifold pressures (i.e.100 psig) the orifice flow characteristics in this transition zone tend to be erratic suggesting instability of the flow. This trend however quickly stabilizes as the manifold pressure is increased. When the flow is erratic it is difficult to define the inception point however it is clear that it is not constant and varies with velocity ratio. At higher manifold pressure in some cases there is a transition zone and when this occurs the inception point is definable and is not a function of velocity ratio. What is causing this erratic behavior is not clear and would require visual observations of the flow as well as additional measurements to better understand.

Understanding this phenomenon is extremely important to rocket engine design since these erratic flow conditions will always occur during startup and if the engine is deep

throttled to a chamber pressure less than ~ 110 psia. However, for this paper since the point of inception is not easily determined when the flow is erratic the inception point is defined at this time only for well ordered flow conditions.

The inception of cavitation for all test conditions indicated a cavitation inception at about K_{cav} of 1.8 ($K_{cav}^{0.5}$ = 1.34). Typical results are shown in Figure 15 and for this case the flowrate was constant with further lowering of the cavitation number. In some instances, however, while the initiation of cavitation occurred at the same value of K_{cav} it was not abrupt but transitioned to a constant C_c value. The flowrate also did not become constant until the C_c became constant. The transition occurred between K_{cav} of 1.75-1.8.

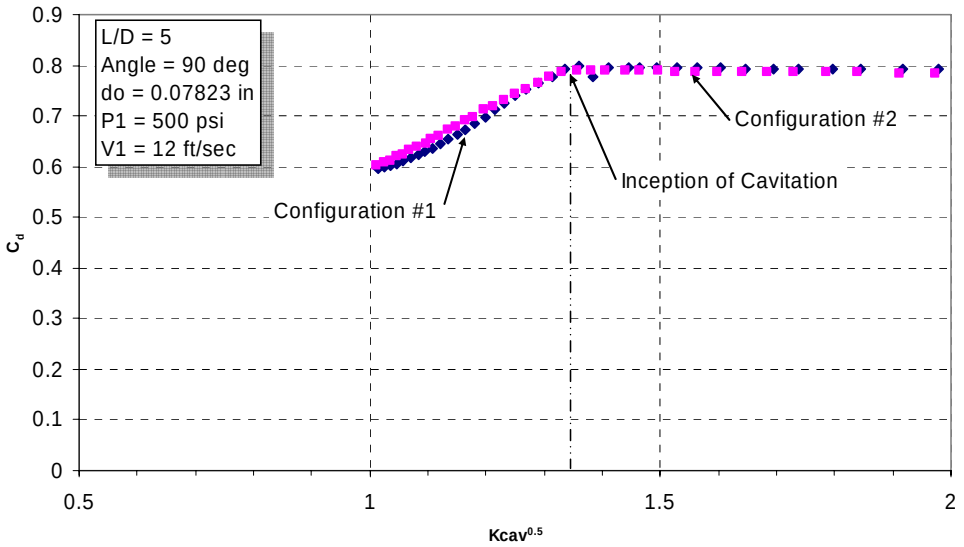

Figure 15 – Illustration of Inception of Cavitation for Configuration #1 and #2

The cavitation number inception for Configuration #3 did not measurably change with cross flow from that found for the other configurations although the transition is less pronounced. This is shown in Figure 16 where the transition was between a cavitation number of 1.8 to 1.75 ($K_{cav}^{0.5}$ between 1.32-1.35).

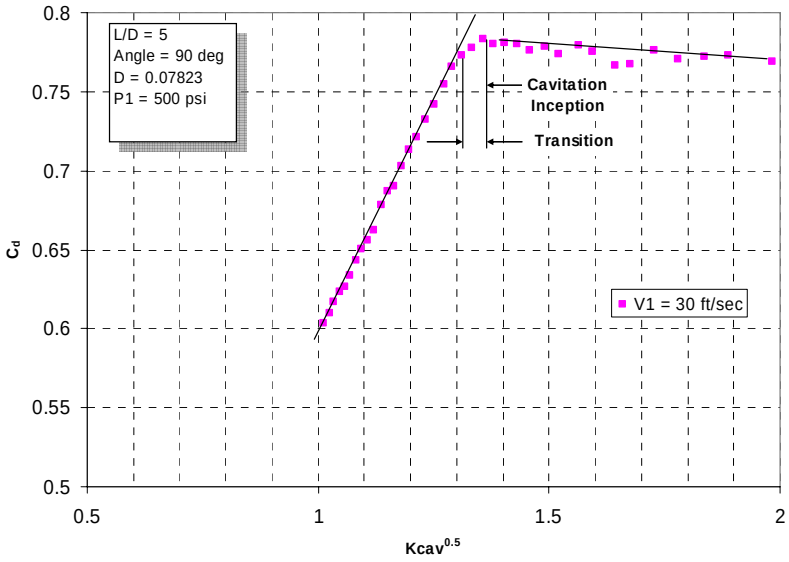

Figure 16 - Cavitation Inception and Transition Region to Full Cavitation

It is interesting that at the point of inception of cavitation the flowrate is still not constant, as shown in Figure 17, until the cavitation number reaches the point where C_c is constant ($K_{cav}^{0.5} \sim 1.28$). This finding is extremely important in that it suggests that the orifice is not choked as previously hypnotized by others until full cavitation is reached.

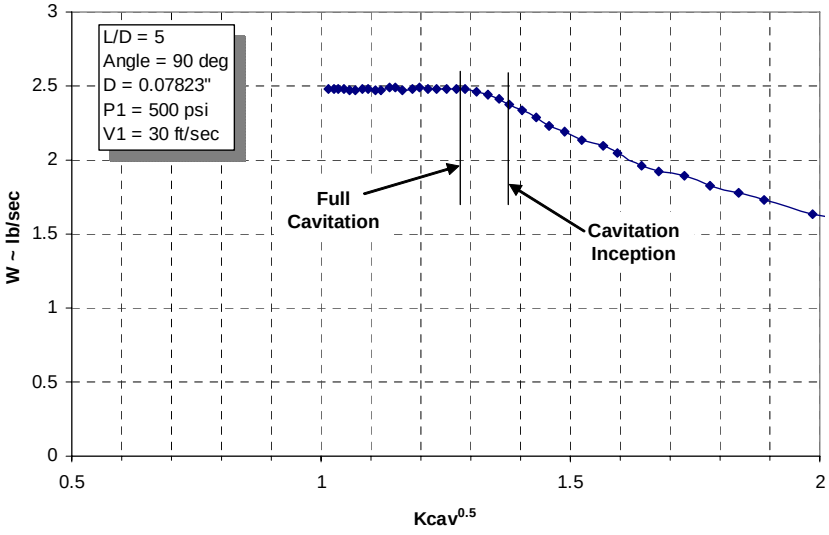

Figure 17 - Cavitation Impacts on Flowrate

It should be noted that Mishra and Peles[17] and Yan[20] determined that the amount of dissolved oxygen in the fluid changed the value of K_{cav} where the inception of cavitation occurred. The Mishra and Peles study for micro channels showed that inception ranged from 1.2 to 1.6 as the concentration varied from 2 to 15 PPM. They also noted that the transition in the flow regimes from incipient cavitation and then to choked flow was rapid. The amount of dissolved gases in the water used in the tests of our study was not measured, however the water used in the tests was stored for long periods of time in air at atmospheric temperature and pressure, so it is reasonable to assume the amount of dissolved gases was near the equilibrium value, which for nitrogen at 298K is 23 PPM. The equilibrium value increases substantially as the water is pressurized. Care was taken that the water did not spend long periods of time in a pressurized state before a test. In addition, the piping configuration ensured a slug flow condition, so any increase in dissolved gases during pressurization would have been limited to a region near the gas / liquid interface in the tank, due to the slow rate of diffusion. Therefore, it is reasonable to assume that the amount of dissolved gases in the water actually flowed through the orifice was that of the equilibrium unpressurized state. The observed K_{cav} value of 1.8 at cavitation inception is therefore not inconsistent with the results of Mishra and Peles.

For the configurations studied, within experimental accuracy, the inception of cavitation was found to occur at the same value. This was compared with that predicted by the relationship[21]:

$$Kincept = 1.9(1 - r/D)^2 - \frac{1000}{\mathrm{Re}\,h} \qquad (18)$$

Where for our study r/D = 0.003 and Reh is the "head" Reynolds Number defined as:

$$\mathrm{Re}\,h = D\rho/\mu\sqrt{2g(P_1 - P_2)/\rho} \qquad (19)$$

Applying values from this study the K_{incept} is 1.88 which is close to that experimentally determined and is certainly within the accuracy of the data (K_{cav} = 1.8).

FULL CAVITATION (CONSTANT FLOWRATE & C_c)

At cavitation the pressure in the vapor cavity is below the vapor pressure then rises as the flow expands to a pressure greater than the back pressure at reattachment. The flow then slowly drops to the back pressure at the orifice exit. The pressure variation throughout the orifice length for the core and near wall flow is illustrated in Figure 18. Full cavitation is defined as the condition where the flowrate and C_c become constant and the attachment point has not reached the orifice exit.

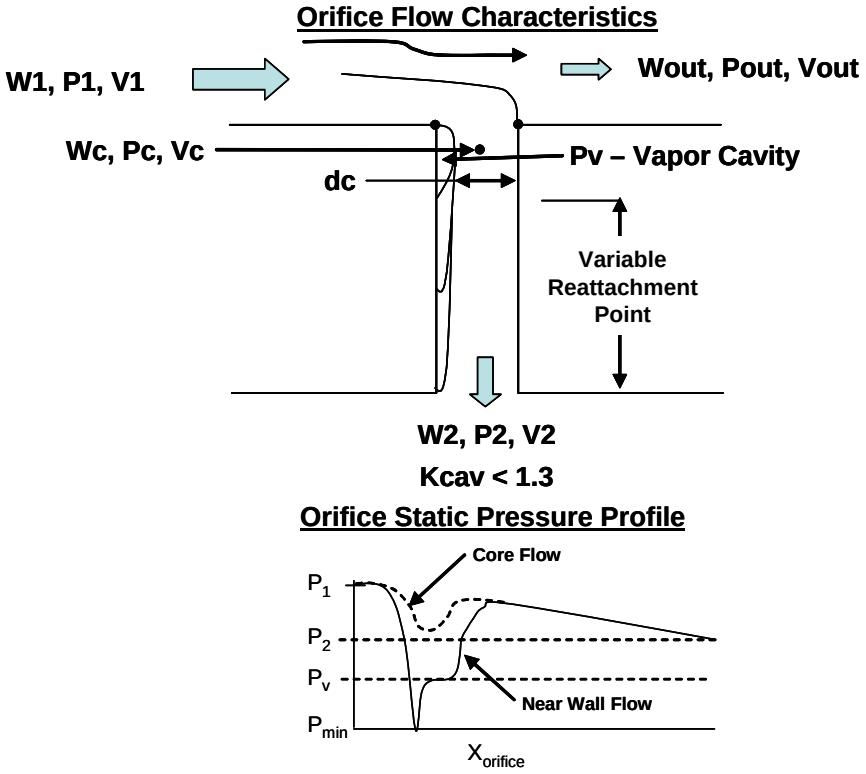

Figure 18 - Static Pressure Characteristics at Cavitation

As the back pressure is lowered (P_2 approaching P_v) the contraction coefficient remains constant but the attachment point moves toward the orifice exit[4, 15 and 18]. In the limit, it has been observed that the attachment is at the orifice exit. During this process the flow at the vena-contracta is "choked" and the back pressure no longer influences the flow parameters upstream of the vena-contracta. Since C_c is constant at full cavitation the area of the vena-contracta also remains constant.

As the expansion process progresses droplets form in the vapor pocket, are re-entrained in the bulk flow, and new droplets formed. The amount of droplets in the vapor pocket increase as the reattachment point approaches the orifice exit.

If the orifice length is insufficient to meet the length required for reattachment between the onset of cavitation and a cavitation number of 1, then one of two conditions occur. If the flow is unable to reattach then the flow will experience separation (hydraulic flip). If the flow does not separate, then the unsteady nature of the flow at separation results in vapor and water exiting the orifice. As discussed in the Supercavitation section of the paper, a vapor cloud surrounding the core liquid has been observed and photographed by other researchers.

In Figure 19 the results of Sato and Saito[19] for L/D of 4.5 illustrates the relationship between cavitation number and cavity extent in the orifice. It should be noted that for consistency Saito's definition of cavitation number was converted to the definition used

in this paper. These results are extremely interesting in that they show that the cavity reaches the exit of the orifice at a cavitation number of ~1.7. Sato's data for Configuration #1and L/D of 2.2 shows that full flow occurs at a cavitation number of 1.7, and that decreasing the orifice size significantly increases the cavitation number for full flow. Also of interest is that once the cavity reaches about ¼ of the orifice length the cavity reattachment instantly "jumps" to the orifice exit. This type of dramatic change is mirrored in Figure 7 where C_d dramatically decreases then becomes near constant.

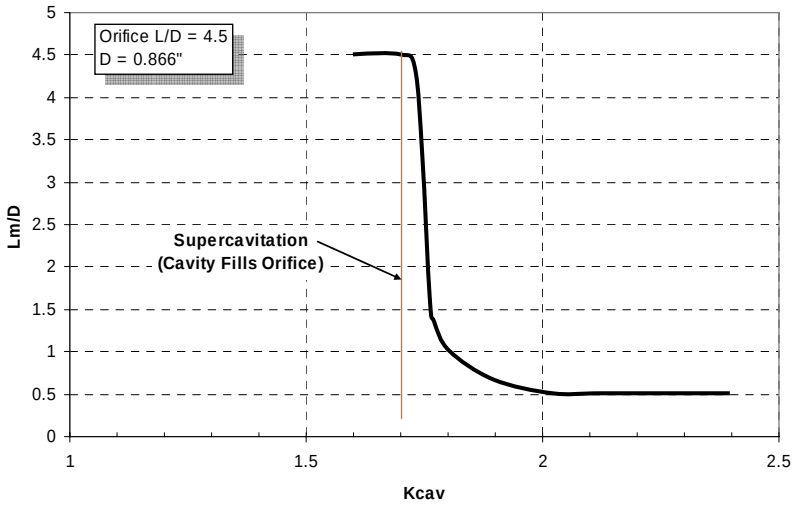

Figure 19 - Relationship between K_{cav} & Cavity Extent[19]

Full cavitation occurs for Configurations #1 and #2 at a K_{cav} of about 1.7-1.75. The results, as indicated in Figure 20, clearly show that the vena contracta between Configuration #1 and #2 are identical with C_c (0.615). These values are reasonably close to Sato's results considering the difference in the orifice diameter.

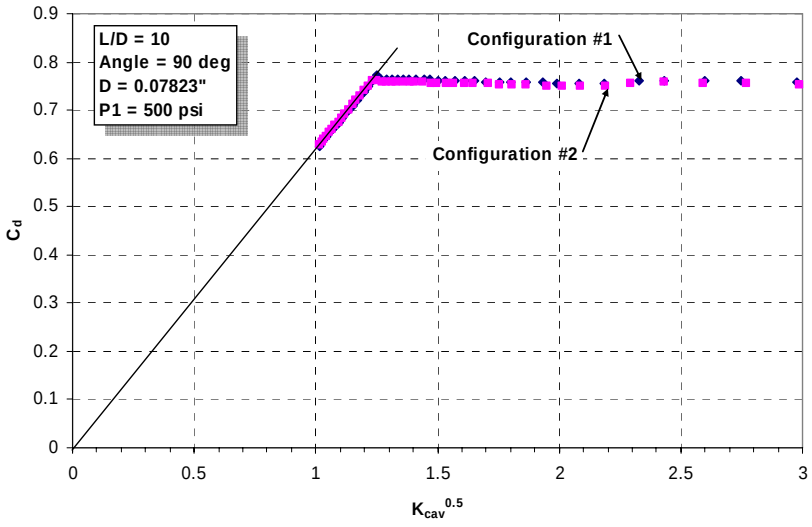

Figure 20 – Comparison of Cavitation Characteristics, Configurations #1 and #2

This suggests that while there is a significant difference between the cavity characteristics, it does not impact C_c (i.e. A_c). Note that in all cases the flow is attached and cavitation remains to at least a value of K_{cav} = 0.996. It should be noted that the minimum back pressure was 0.042 psig. For this orifice design the expected C_c is determined from[2]:

$$C_c = \frac{1}{\sqrt{\frac{1}{0.611^2} - 11.4\frac{r}{D}}} \qquad (20)$$

For the orifices used in this study r/D is < .003 resulting in a value of C_c of 0.615. Configuration #1 experimentally determined value compares with that determined from Equation 20. Also, the experimentally determined C_d of 0.76 compares well with the data of Licharowicz[3] (0.75).

As indicated in Figure 21 the relationship between C_d and C_c, K_{cav} is still linear even with cross flow.

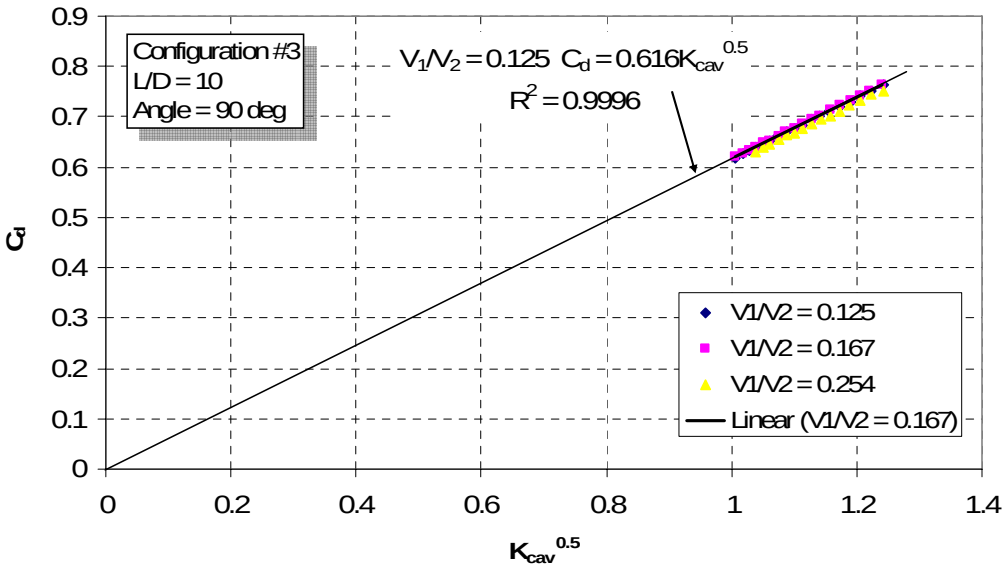

Figure 21 - Constant Contraction Coefficient in a Sharp Edge 90 degree Orifice

Results shown in Figure 22 validate that when C_c is constant the flowrate is also constant. This is similar to that of a cavitating venturi.

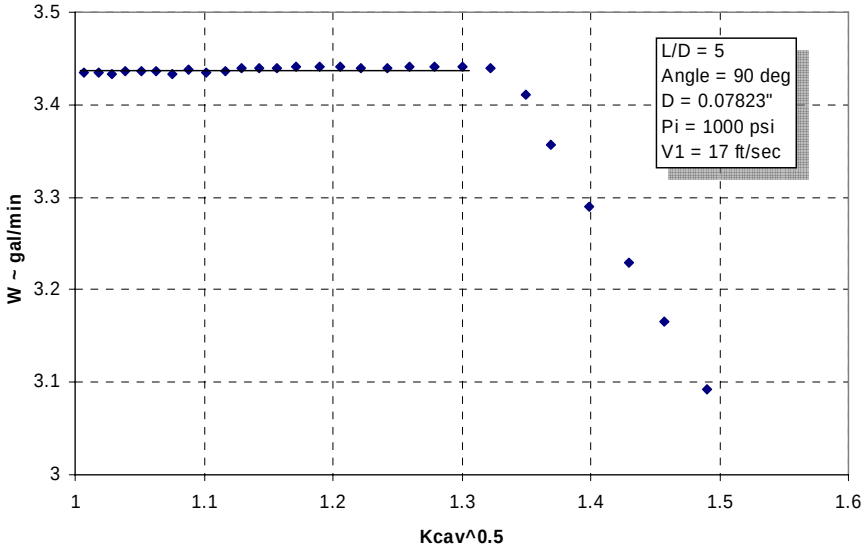

Figure 22 - Illustration of Constant Flowrate in the Cavitation Regime

Inspection of Equation 13 shows that the data analysis for Cc is at constant A_1/A_2, V_1/V_2, and L/D. Therefore, the calculated C_c may be independently a function of these variables:

$$C_c = f\left(A_1 / A_2, V_1 / V_2, L / D\right) \qquad (21)$$

From a physical basis the area ratio should only impact the flow contraction and L/D would only impact the expansion, turbulence, and friction losses flow downstream of the vena-contracta. The independent impact of velocity ratio should also impact head loss. These losses all impact the overall head loss and if significant would result in an independent impact on Cc.

To test these variables the data are plotted in Figures 23, 24, and 25 as function of velocity ratio and area ratio for a specific L/D. The results show that at L/D of 10, C_c is not a function of area ratio although as the L/D decreases there is an indication of a minor impact. This is the result of the flow not following the constant C_c characteristic at the lower value of L/D suggesting that the flow is being impacted by other processes not included in the original derivation. If the L/D characteristics are compared there is also indication of an independent impact although the variation is within the overall experimental error. Note, also that Cc tends to decrease as the velocity ratio is increased beyond ~ 0.45. For velocity ratios greater than about 0.5 represents the data obtained at an upstream pressure of 100 psi, which again is in the flow conditions where the flow was not well behaved. It is possible that these variables have an independent impact, however sufficient measurements were not taken to identify what is causing the flow behavior in the low upstream pressure and short L/D.

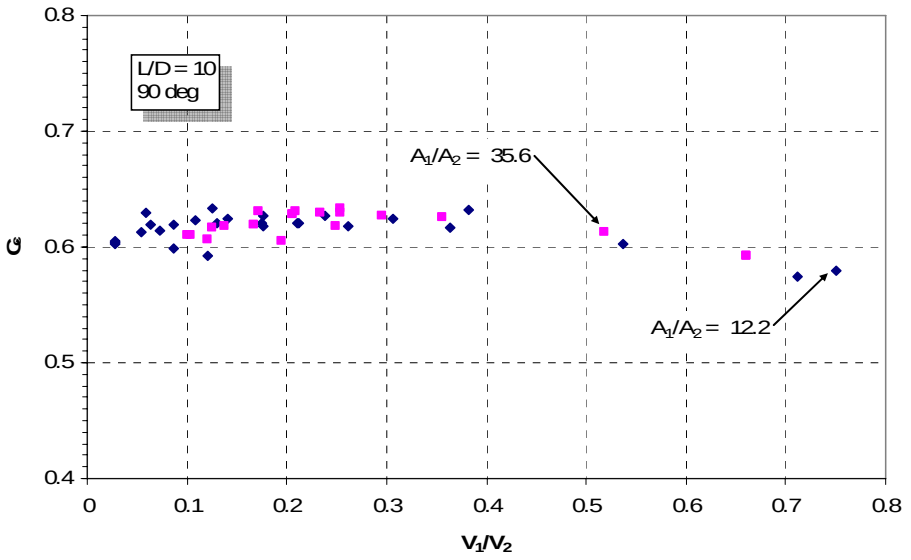

Figure 23 – Impact of Area Ratio and Velocity Ratio on C_c for L/D = 10

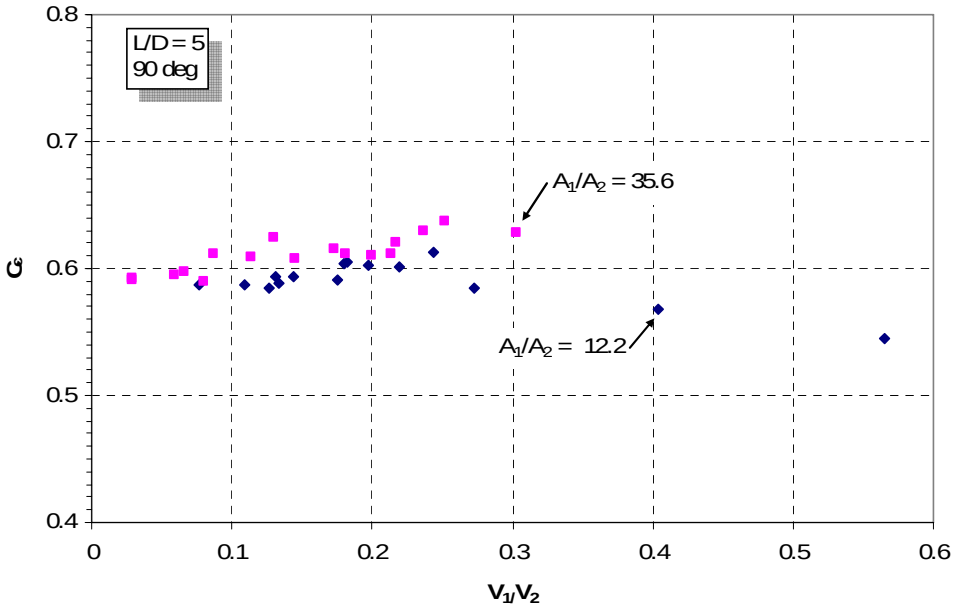

Figure 24 - Impact of Area Ratio and Velocity Ratio on C_c for L/D = 5

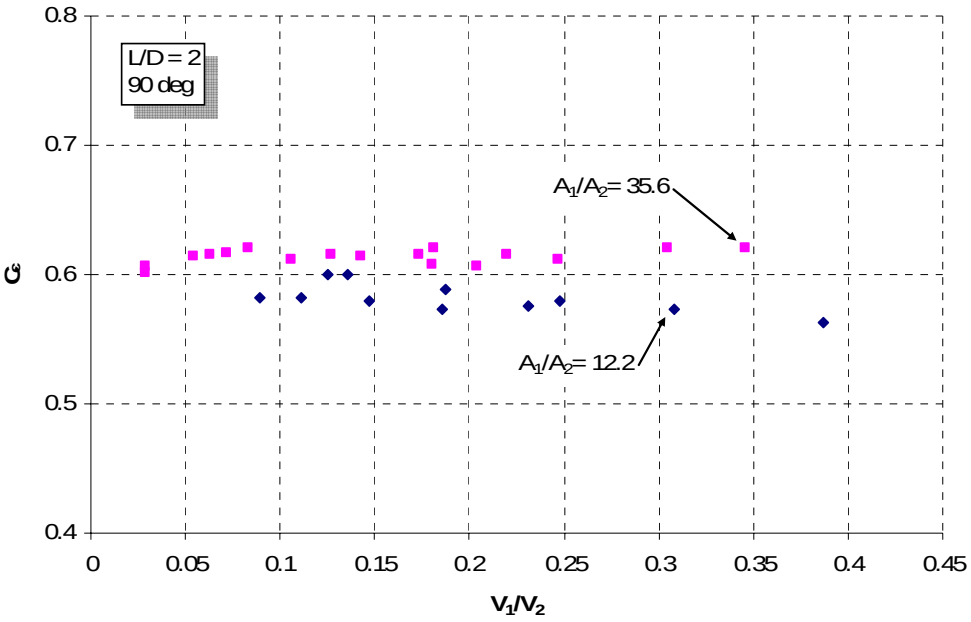

Figure 25 - Impact of Area Ratio and Velocity Ratio on C_c for L/D = 2

For well behaved flow conditions Equation 13 provides excellent prediction of the contraction coefficient. However, for conditions where the flow may be less well behaved Figures 23-25 provide an estimate of the additional impacts. The development of a complete correlation requires additional data with emphasis in the low upstream pressure range and L/D less than 5.

SUPERCAVITATION

Chaves et al[15] defines supercavitation to describe when the cavities extended past the exit of the nozzle but the orifice does not experience separation and the spreading jet is surrounded by a vapor cloud as indicated in Figure 26. Chaves also noted that supercavitation was accompanied by a dramatic increase in the spray angle produced by the nozzle. Visual observations[7] of cavitation flows in nozzles have, in addition, shown a transient behavior caused by quasi-periodical re-entrant jet motion in the vena-contracta region, and random collapse of the cavitating bubbles at the nozzle exit.

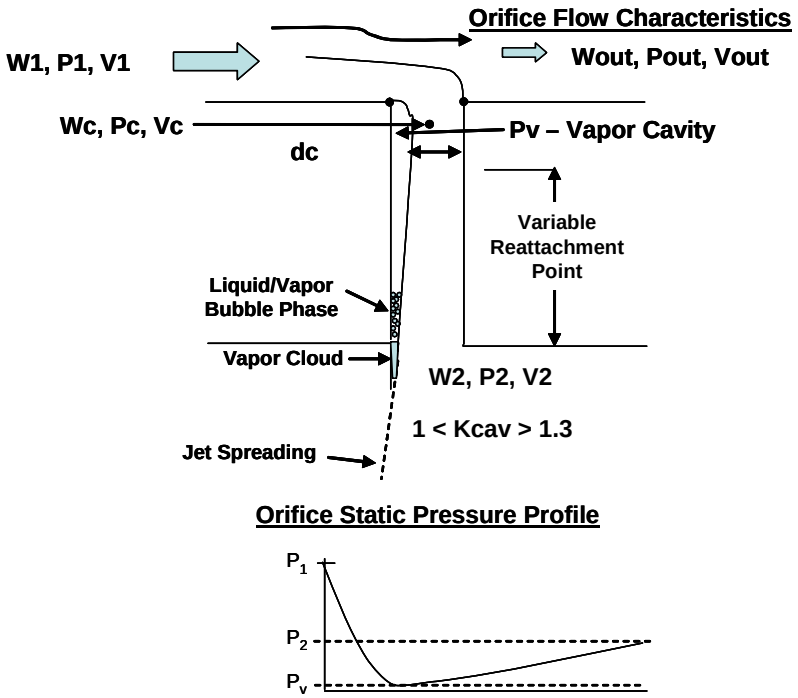

Figure 26 - Illustration of Supercavitation Jet Characteristics

The two-phase bubble nature of cavitation flows has been confirmed by measurement and visualization[7, 8, 15 and 19]. At this condition the flow is no longer choked and C_d experiences either a dramatic step decrease followed by more gradual lowering (as the back pressure is further lowered) until the minimum is reached or complete separation allowing the back pressure to surround the jet from the orifice exit to the vena-contracta.

Koivula's[8] results in this regime show that, due to the implosion of vapor in the cavity which produces shock waves, the frequency of oscillations decrease from 8 KHz at inception of cavitation to ~700 Hz at supercavitation and the overpressure increases to as high as $\pm$ 90 psi.

In tests utilizing Configuration #2 with the L/D of 5 orifice, supercavitation occurred at K_{cav} of about 1.6 ($K_{cav}^{0.5}$ = 1.25; see Figure 7) and at this point the discharge coefficient dropped dramatically. Upon further reduction the decrease in C_d tended to reach a constant value equal to that of separation. Ahn et al[5] also noted that for an L/D of 5 and orifice size of 0.04" as the cavitation number is increased the flow transitions very quickly from separated flow to cavitating flow similar to that shown in Figure 7.

The data in Figure 27 compares the Configuration #1 and #2 cavitation characteristics. For Configuration #2 C_c is constant in the cavitation regime while for Configuration #1 supercavitation occurs as noted by the variation from the linear curve.

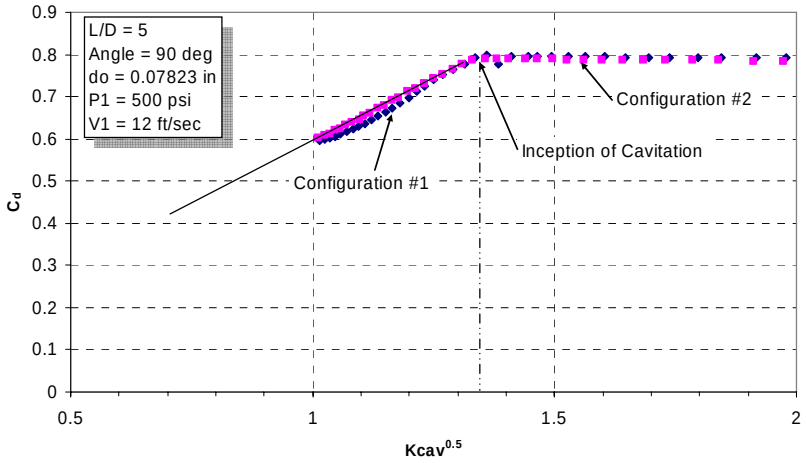

Figure 27 - Illustration Showing the Gradual Onset of Supercavitation

The experimental data confirm that the flow is not constant in the supercavitation regime suggesting that the cavity is no longer choked as shown in Figure 28. This is similar to the onset of cavitation where the flowrate varies but returns to the prior value corresponding to that at cavitation.

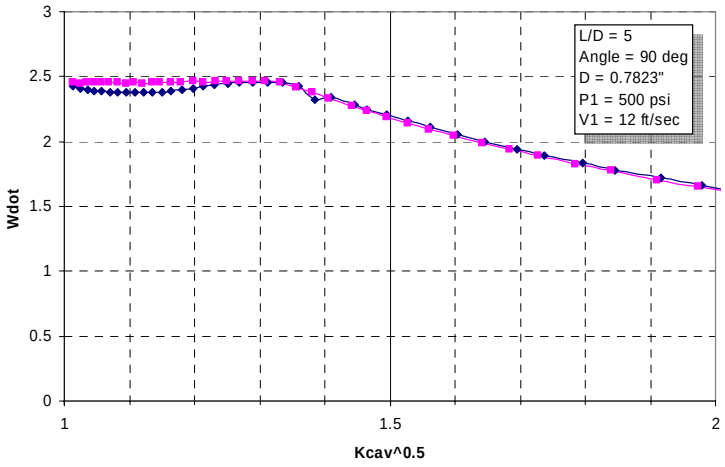

Figure 28 - Variable Flowrate in the Supercavitation Regime

One explanation for the variation in flowrate is that the pressure oscillations at the orifice exit caused by the unsteady re-entrainment process results in the cavitation number varying sufficiently that the flow varies between cavitation inception, cavitation, or the non-cavitation regimes. For our experiments no high speed instrumentation was utilized in these experiments to determine the magnitude and/or frequency of the oscillations. However, considering the magnitude of overpressure measured by Koivula[8], the flowrate

could easily vary from 0 to choked flow to separation at very high frequencies. The mean flowrate of course would be lower than that of choked flow similar to that shown in Figure 18. Also the high/low overpressure combined with the very high frequencies could account for the vapor leaving the orifice and not allowing the back pressure to enter the orifice. This is an area that requires additional study and experimentation.

The cross flow results tended to be less impacted by supercavitation then the other configurations. In Figure 29 the Configuration #3 data where velocity ratio was varied show that supercavitation did not occur. This is contrasted with Figure 27, Configuration #2.

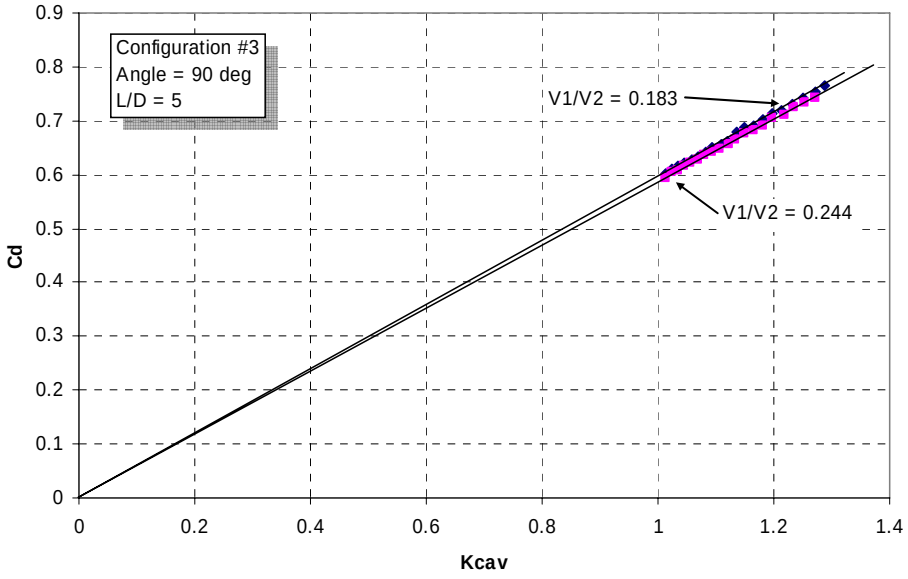

Figure 29 – Configuration #3 Cross Flow Impacts on Supercavitation

SEPARATION (HYDRAULIC FLIP)

Separation occurs when the acceleration forces at the entrance to a sharp-edge orifice are sufficient to cause the flow to fully detach from the wall and the orifice L/D is insufficient to allow for reattachment. An illustration of separation is provided in Figure 30.

For the case where the flow fully separates the C_d will immediately decrease to the minimum value and remain there as the back pressure is lowered. An example of the dramatic drop in C_d at separation then a near constant C_d as the cavitation number approaches 1 is shown in Figure 31. As stated above the initiation occurs at $K_{cav}^{0.5} \sim 1.25$ (cavitation umber of ~1.6). The variation in C_c in the cavitation regime is due to the velocity ratio impacts as discussed above.

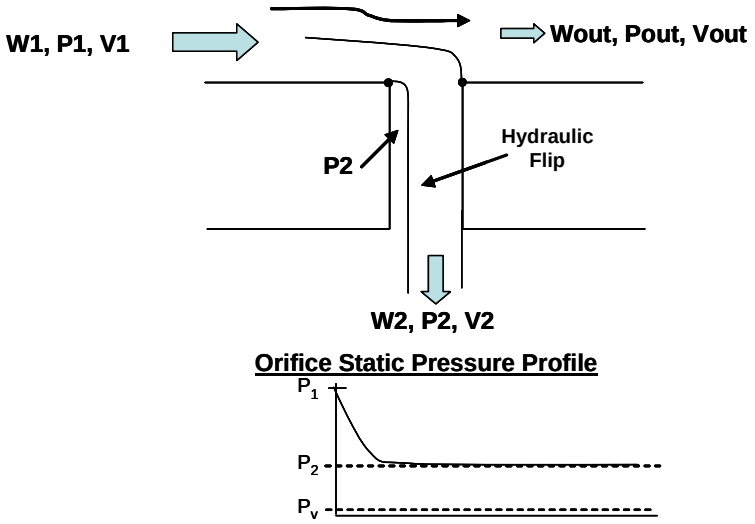

Figure 30 - Illustration of Separation (Hydraulic Flip)

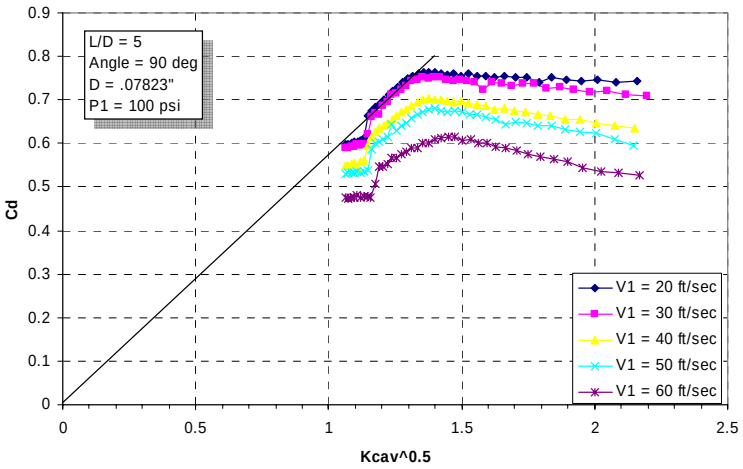

Figure 31 - Flow Characteristics Illustrating Separation

The variation in orifice flowrate for the 60 ft/sec data is shown in Figure 32. These results show that the flow is constant in the cavitation regime then experiences a step change in flowrate at the onset of supercavitation, and then continues to vary as the cavitation number approaches 1. Further note the large shift in flowrate rather than the gradual change that is observed in the supercavitation regime.

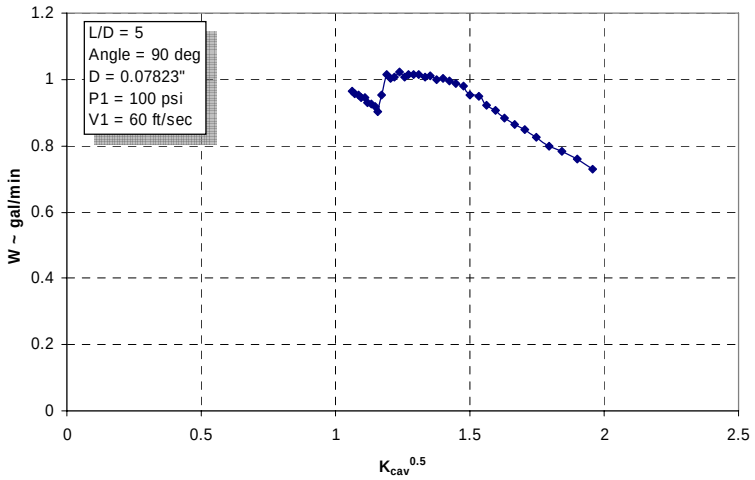

Figure 32 - Illustration of Flowrate Variation at Separation

A relationship for the critical cavitation number for hydraulic flip[21] is:

$$Kcrit = 1 + \frac{1}{(1 + L/4D)(1 + 2000/\mathrm{Re}\,h)e^{70r/D}} \qquad (22)$$

The results from this study are compared with the predictions from Equation 22 in Figure 33. Note the excellent agreement. The L/D of 10 for the 0.07823 inch orifice does not fit the correlation since it did not experience separation within the range of this study. However, the smaller orifice did experience separation and correlates well with the prediction. Equation 22 is stated to be valid only for short L/D orifices[21], and these results suggest that the limit is about L/D = 10.

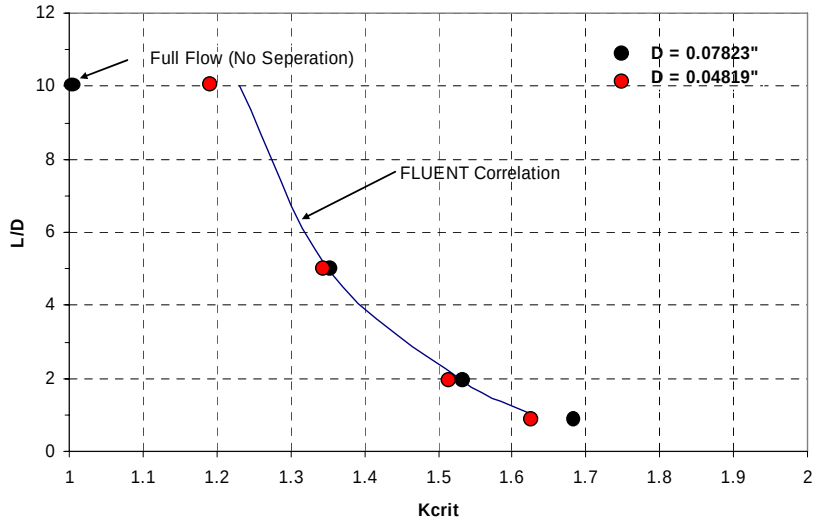

Figure 33 - Comparison of measured Separation with Equation 22 Correlation[21]

The contraction coefficient at separation is shown in Figure 34. The correlation should be used with caution since the range of the parameters is limited. The resulting equation is:

$$C_c = -0.1054\frac{V_1}{V_2} + 0.6158 \qquad (23)$$

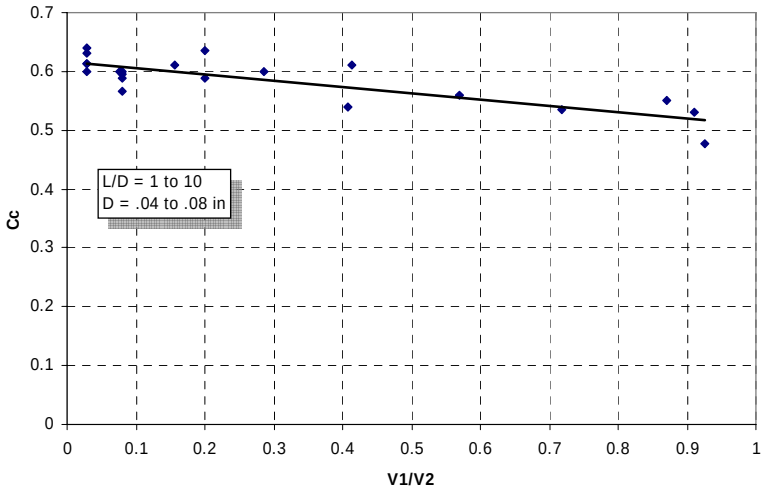

Figure 34 - Contraction Coefficient vs Velocity Ratio at Separation

CONCLUSIONS

The results presented clearly show the complexity of possible flow conditions for sharp-edge orifices in cross flow. For example, an orifice can initially flow separated then either (1) quickly attach in the cavitation regime, (2) attach in the non-cavitation regime, or (3) remain separated regardless of flow conditions. The ability to select which scenario the orifice will be operating in ***is the challenge***. Once this is selected then all pertinent flow parameters can be defined.

The most significant contribution of this study is the extension of the linear cavitation model verified in numerous studies to include both cavitation and non-cavitation flows with 3 manifold fluid feed configurations. The supporting relationship provides design engineers with the ability to more knowledgably predict flow regimes as well and flow variables for determination of $C_{c,}$ C_d and $K_{L.}$.

In the non-cavitation regime the results of this study show that the head loss can be as high as 8 times that for no cross flow depending on the magnitude of the cross flow. This emphasizes to the design engineer the need to keep the cross flow velocity low to minimize pressure requirements. In addition the data indicate that the major head loss in the non-cavitation regime occurs upstream of the vena-contracta.

The inception of cavitation and the transition to full cavitation has been identified. However, additional studies are required to quantify the variables impacting the transition

from initiation of bubbles to the full cavity formation. Visual studies have also identified the transition and have shown that it can transition to full cavity very rapidly. No correlations have been offered to date.

In the cavitation regime the validity of the first order relationship was shown to be related to the fact that the head loss from the manifold to the vena-contracta is small. Cross flow impacts C_c revealing the significance of cross flow velocity on the vena-contracta formation process.

This study has determined that the flow is not choked in the supercavitation regime. It is postulated that this is related to the unsteady nature of the flow (frequency and overpressure). In addition the onset of supercavitation is not defined sufficiently so that with certainty a prediction that it will occur and further, when it occurs, will it immediately cause separation or quasi-attachment until separation occurs. The results of this study can only determine that once supercavitation occurs it CAN cause immediate separation or quasi separation as back pressure is further lowered. Additional studies are required to better define where supercavitation will occur by defining the conditions that cause the cavity to grow and suddenly jump to the orifice exit and then the change in the processes occurring at the exit leading to separation. Of particular interest to rocket engine injector design is the potential for the unsteady nature of supercavitation to trigger combustion instability in the combustion chamber especially during startup.

The impact of L/D for sharp-edge 90 degree orifices has been defined and the data was correlated with an existing correlation predicting separation with short L/D orifices. This correlation, however, can only predict that separation is likely to occur.

NOMENCLATURE

SYMBOLS

A	Area in^2; Constant in Equation
B	Constant in Equation
C	Constant in Equation
C_c	Contraction Coefficient, A_2/A_1
C_d	Discharge Coefficient
D	Orifice Diameter, in
H_L	Head Loss, lb/in^2
K	Loess Coefficient
K_{cav}	Cavitation Number
L	Orifice Length, in
P	Pressure, psi, psia
Re	Reynolds Number
r	Orifice Entry Radius, in
V	Velocity, ft/sec
W	Flow Rate, lb/sec

GREEK

ρ	Liquid Density, lb/ft^3

SUBSCRIPTS

1	Manifold
2	Orifice Exit
a	Contraction
c	Contraction
crit	Critical at Separation
h	Head
incept	Cavitation Inception
v	vapor
out	Exiting Manifold
turb	Turbulence
f	Friction

REFERENCES

1. Strakey, P. A. and Talley, D. G., "The Effect of Manifold Cross-Flow on the Discharge Coefficient of Sharp=Edged Orifices" Atomization and Sprays, Vol. 9, No 1, Jan 1999
2. Nurick, W. H., Orifice Cavitation and Its Effects on Spray Mixing, Journal of Fluids Engineering, *page 98, 1976.*
3. Ganippa, G., Bark, G., Andersson, S. and J Chomiak, Computer Aided Verification, (CAV) 2001, Session A9.005, Paris, France 2001
4. Lichtarowicz, A., Duggins, R, and E. Markland, Discharge Coefficients for Incompressible Non-Cavitating Flow through Long Orifices, Journal of Mechanical Engineering Science, *7:2, 1965.*
5. Ahn, K., Kim, J., and Y. Yoon, Effects of Orifice Internal Flow on Transverse Injection into Subsonic Crossflows: Cavitation and Hydraulic Flip, Atomization and Sprays, Vol. 16, pp. 15-34, 2006
6. Heiniger, K. C., Introduction to the Flow States in Water Jet Systems, FHA University of Applied Sciences, Krakow, Poland, 15 Nov. 2001
7. Martynov, S., Mason, D., And Heikal, M. "Hydrodynamic Similarity of Cavitation Flows in Nozzles" Proc. 5th International Symposium on Multiphase Flow, Heat Mass Transfer and Energy Conversion, Xi'am, China 3-6 July 2005
8. Koivula, T., On Cavitation in Fluid Power, Proc. Of 1st FPNI-PhD Symposium, Hamburg, Germany, 2000, pp371-382
9. Schmidt, D. P., Rutland, C J., and Corradini, M. L., "A Numerical Study of Cavitating Flow Through Various Nozzle Shapes", SAE Paper 971597, 1997
10. Schmidt, D. P., Rutland, , C J., and Corradini, M. L., "Cavitation in Two Dimensional Asymmetric Nozzles" SAE Paper No. 1999-01-0518

11. Perry and Chilton, Chemical Engineering Handbook, 5th Ed.
12. Fox, R, and McDonald, A, Introduction to Fluid Dynamics, 3rd Edition, Wiley, 1985
13. Dubois, R., MS Thesis, MIT Dept of Civil Engr., 1954
14. Crane, Flow of Fluids through Valves, Fittings, and Pipe, 1976 Tech. Paper, 1976 Ed.
15. Chaves, H., Knapp, M, Kubitzek, A., Obermeier, F, and T. Schneider, Experimental Study of Cavitation in the Nozzle Hole of Diesel Injectors Using Transparent Nozzles, SAE Paper 950290, March 1955
16. Soteriou, C., Andrews, R., and M. Smith, Direct Injection Diesel Sprays and the Effect of Cavitation and Hydraulic Flip on Atomization, SAE Paper 950080, SAE, 1995.
17. Misha, C., and Y. Peles, Cavitation in Flow through a Micro-Orifice Inside a Silicon Microchannel, Physics Of fluids, 17, 013601, 2005
18. Bergwerk, W., Proceedings of the Institution of Mechanical Engineers, 173(21), pp 655-660, 1959
19. Sato, K., and Y. Saito, Unstable Cavitation Behavior in a Circular-Cylindrical Orifice Flow, JSME International Journal, Series B, Vol. 45, No.3, pp638-645, 2002
20. Y. Yan and R. B. Thorpe., "Flow regime transitions due to cavitation in the flow through an orifice," Int. J. Multiphase Flow **16**, 1023 (1990).
21. Fluent Corporation, 19.4.1 Atomizer Models